Journal of Applied Physics

Size effects in the formation of an uncompensated ferromagnetic moment in NiO nanoparticles

Cite as: J. Appl. Phys. **126**, 103904 (2019); https://doi.org/10.1063/1.5109054
Submitted: 08 May 2019 . Accepted: 20 August 2019 . Published Online: 11 September 2019

S. I. Popkov, A. A. Krasikov, A. A. Dubrovskiy, M. N. Volochaev, V. L. Kirillov, O. N. Martyanov, and D. A. Balaev

Journal of Applied Physics ARTICLE scitation.org/journal/jap

Size effects in the formation of an uncompensated ferromagnetic moment in NiO nanoparticles

Cite as: J. Appl. Phys. **126**, 103904 (2019); doi: 10.1063/1.5109054
Submitted: 8 May 2019 · Accepted: 20 August 2019 ·
Published Online: 11 September 2019

S. I. Popkov,[1] A. A. Krasikov,[1] A. A. Dubrovskiy,[1] M. N. Volochaev,[1] V. L. Kirillov,[2] O. N. Martyanov,[2] and D. A. Balaev[1]

AFFILIATIONS

[1]Kirensky Institute of Physics, Federal Research Center "Krasnoyarsk Scientific Center, Siberian Branch, Russian Academy of Sciences," Krasnoyarsk 660036, Russia
[2]Boreskov Institute of Catalysis, Siberian Branch, Russian Academy of Sciences, Novosibirsk 630090, Russia

ABSTRACT

The magnetic properties of samples of NiO nanoparticles with average sizes of 23, 8.5, and 4.5 nm were investigated. Using the magnetization curves measured in strong (up to 250 kOe) pulsed magnetic fields, the contributions of the free spin and ferromagnetic subsystems were extracted. It has been found that the ferromagnetic contribution increases with a decrease in the nanoparticle size and is proportional to the fraction of uncompensated exchange-coupled spins. It is demonstrated that the uncompensated spins form in the antiferromagnetic NiO oxide due to an increase in the fraction of surface atoms in the nanoparticles with decreasing particle size and defects in the bulk of particles.

I. INTRODUCTION

The effect of surface and defects on the magnetic properties of antiferromagnetic (AFM) materials strengthens with a decrease in the size of particles that form these materials. It is well-known that the fraction of surface atoms in particles smaller than 10 nm can attain tens of percent. The surface atoms can be considered defects, which lead, similar to the bulk defects, to the partial decompensation of spins in the ferromagnetically ordered planes; as a result, an AFM nanoparticle acquires the magnetic moment. Néel[1] used a statistical approach to estimate the uncompensated magnetic moment of such a particle,

$$\mu_p \sim \mu \cdot N^{\mathbf{b}}. \quad (1)$$

Here, N is the number of magnetically active atoms in a particle and μ is the magnetic moment of an atom. Depending on the defect type, the exponent **b** takes different values: **b** = 1/3 for defects on the particle surface, **b** = 1/2 for defects both on the surface and in the bulk of a particle, and **b** = 2/3 at the uneven number of planes with parallel spins in a particle. The μ_p value is significant when the number of atoms N is smaller than $\sim 10^4$, i.e., in particles about 10 nm in size and smaller.[2,3] Therefore, small AFM particles become ferromagnetic (FM) in the sense of forming a FM subsystem related to the partial decompensation of spins against the background of the AFM ordering. This property broadens the range of possible applications of AFM nanoparticles in different fields.[4–6]

To determine the uncompensated magnetic moment μ_p of a particle and related characteristics, it is necessary to know the size distribution of synthesized particles in an ensemble and their behavior in different magnetic fields. Thus, the analysis of the observed magnetic properties of disperse samples makes it possible to establish a defect type (surface or bulk) in nanoparticles and relate the obtained characteristics to the synthesis conditions and crystallochemical properties of a material. For instance, it was established for AFM-ordered ferritin and ferrihydrite on the basis of numerous investigations[6–16] that it is the surface and bulk defects that lead to the occurrence of the uncompensated magnetic moment: Eq. (1) is valid at the **b** value similar to 1/2. In other AFM materials, similar estimations did not yield an unambiguous picture; the exponents **b** in Eq. (1) were different.[17–22]

The AFM nanoparticles contain, along with the AFM-ordered core, the FM subsystem and the subsystem of spins uncoupled with the AFM core, which exhibits the spin-glass-like behavior in the low-temperature region.[22–32] For this reason, it is difficult to extract the magnetic contribution of each phase.[11,27,33–36] In this study, we demonstrate a way of separating the contributions of the above-mentioned magnetic subsystems using the measurements of magnetization in strong pulsed magnetic fields. The objects of this study were samples of AFM nickel oxide (the Néel temperature of bulk NiO is ~523 K) with average particle sizes of 23, 8.5, and

4.5 nm. The basic idea is that the saturation of the FM subsystem can be unambiguously separated in a strong magnetic field, whereas the response of other magnetic subsystems, i.e., the AFM core and exchange-uncoupled spin subsystem, is field-linear. Thus, the proposed technique yields meaningful data about the magnetic structure and characteristics (μ_p and saturation magnetization) of AFM nanoparticles.

II. EXPERIMENTAL

A. Synthesis of NiO nanoparticles

NiO nanoparticles more than 20 nm in size were synthesized by thermal decomposition of nickel hydroxocarbonate $NiCO_3 \cdot 0.18Ni(OH)_2 \cdot 0.50H_2O$ [nickel carbonate (pure)]. The heating cycle included 14 h at 90 °C, the temperature rise to 500 °C for 5 h, and annealing at 500 °C for 1 h.

NiO nanoparticles several nanometers in size were synthesized by thermal decomposition of nickel oxalate $NiC_2O_4{\cdot}2H_2O$ obtained from $NiSO_4{\cdot}7H_2O$ and $(NH_4)_2C_2O_4{\cdot}H_2O$ taken in the stoichiometric ratio: 14% solution of $NiSO_4{\cdot}7H_2O$ was added to 3.6% solution of $(NH_4)_2C_2O_4{\cdot}H_2O$ under permanent stirring at a rate of 250 rpm for 20 min. The obtained light green precipitate was filtered through a paper filter with a pore diameter of 1–2.5 μm and washed from $(NH_4)2SO_4$ with distilled water. Decomposition was performed in a special temperature mode, which includes the temperature rise from 25 to 400 °C for 40 min followed by 10-min annealing at this temperature. This procedure yielded NiO nanoparticles with an average size of 8.5 nm. To obtain smaller NiO nanoparticles, the nickel oxalate synthesized using this procedure was subjected to ultrasonic treatment in dimethyl sulfoxide (one-to-one mass ratio) before annealing.

Commercial high-purity NiO powder was taken as the reference bulk sample. For magnetic measurements, the powder was compacted as a pellet and annealed at 600 °C. The samples are hereinafter referred to as 23 nm, 8.5 nm, and 4.5 nm, according to the transmission electron microscopy (TEM) data (Sec. II B), and bulk NiO.

B. Characterizing nanosized NiO

X-ray diffraction (XRD) patterns of the NiO nanoparticle samples were obtained on a Bruker D8 Advance (Germany) diffractometer (CuKα radiation, $\lambda = 1.5418$ Å). The XRD patterns are shown in Fig. 1. All diffraction peaks correspond to the NiO phase (PDF no. 047-1049). The NiO cubic unit cell parameter is consistent with a reference value (sp. gr. Fm3.m, $a = b = c = 4.176$ Å, $\alpha = \beta = \gamma = 90°$). The average size of the coherent scattering region of crystallites calculated from the XRD peak half-widths using the Scherrer equation was around 30, 8, and 4.8 nm for the investigated samples.

Figure 2 presents transmission electron microscopy (TEM) images obtained on a JEOL JEM-2010 at an accelerating voltage of 200 kV and the corresponding size distribution of NiO particles. The average particle sizes were found to be 23, 8.5, and 4.5 nm. This is in good agreement with the coherent scattering region calculated using the XRD data.

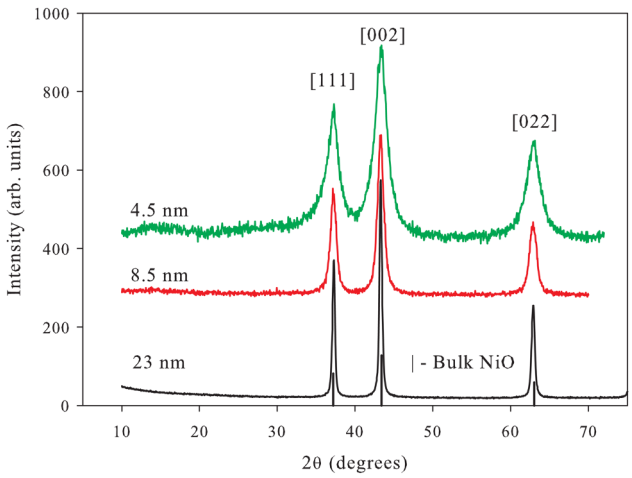

FIG. 1. XRD patterns of the NiO nanoparticle samples. Lines show the positions and relative intensities of the bulk NiO peaks.

C. Magnetic measurements in different field ranges

The quasistatic magnetic measurements were performed on a vibrating sample magnetometer (VSM). The powder was fixed in a measuring capsule in paraffin. The temperature dependences of magnetization M(T) were determined in the zero field cooling (ZFC) and field cooling (FC) modes. In addition, we measured the M(H) dependences on a VSM in fields up to 60 kOe at the temperatures of measurements of the magnetization curves in pulsed magnetic fields.

The measurements of the M(H) curves in pulsed magnetic fields were performed on an original facility at the Kirensky Institute of Physics, Siberian Branch, Russian Academy of Sciences (Krasnoyarsk, Russia). A sample to investigate was fixed in an induction sensor of the pulsed magnetometer. The pulse length was 16 ms. The M(H) isotherms were measured at a temperature of 77 K and a magnetic field pulse amplitude up to 250 kOe. The M(H) dependences described in Sec. III include the data obtained on the pulsed magnetometer in the range of 0–250 kOe and on the VSM in fields up to 60 kOe.

III. RESULTS AND DISCUSSION

Figure 3 shows temperature dependences of magnetization for the investigated samples obtained in the ZFC and FC modes in an external magnetic field of 1 kOe. It can be seen in Fig. 3(c) that the magnetizations of bulk NiO (data for the bulk NiO sample are in good agreement with results obtained in Ref. 37 and coarse (23 nm) nanoparticles differ by a factor of about two. In smaller particles [Figs. 3(a) and 3(b)], the magnetization increases by two–three orders of magnitude. It means that with a decrease in the particle size, the contribution of additional subsystems forming in nanoparticles becomes significant against the background of the magnetic response of the AFM core (similar to bulk NiO).

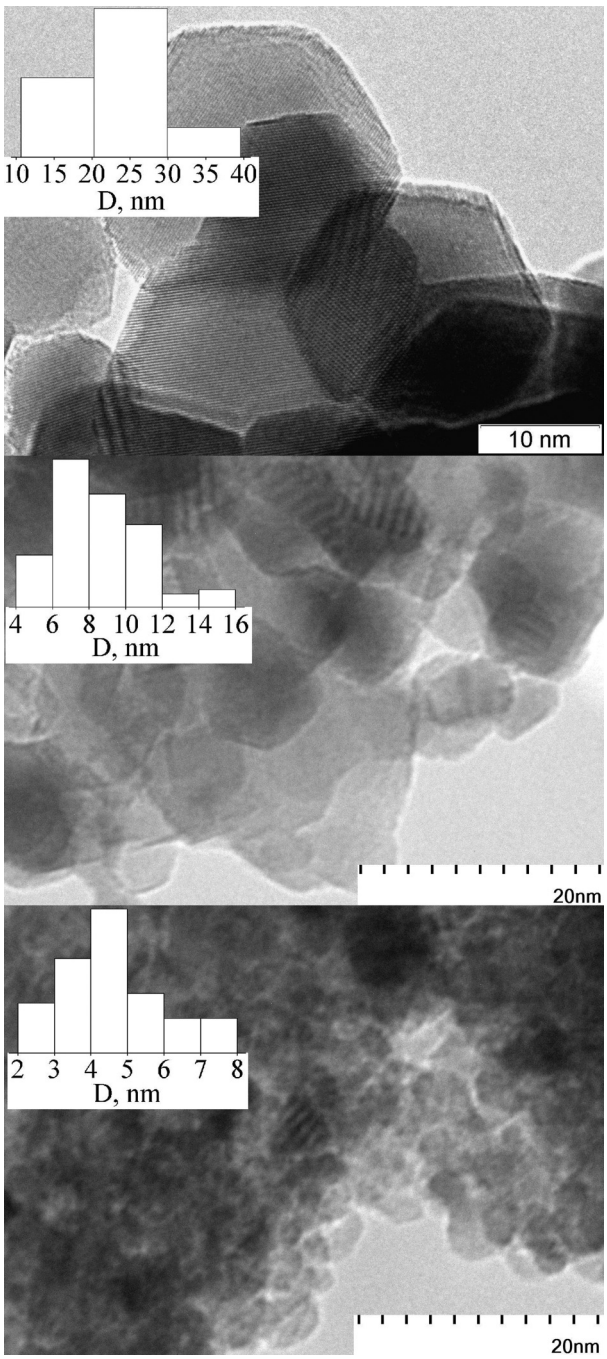

FIG. 2. TEM images and particle size distribution for the investigated samples.

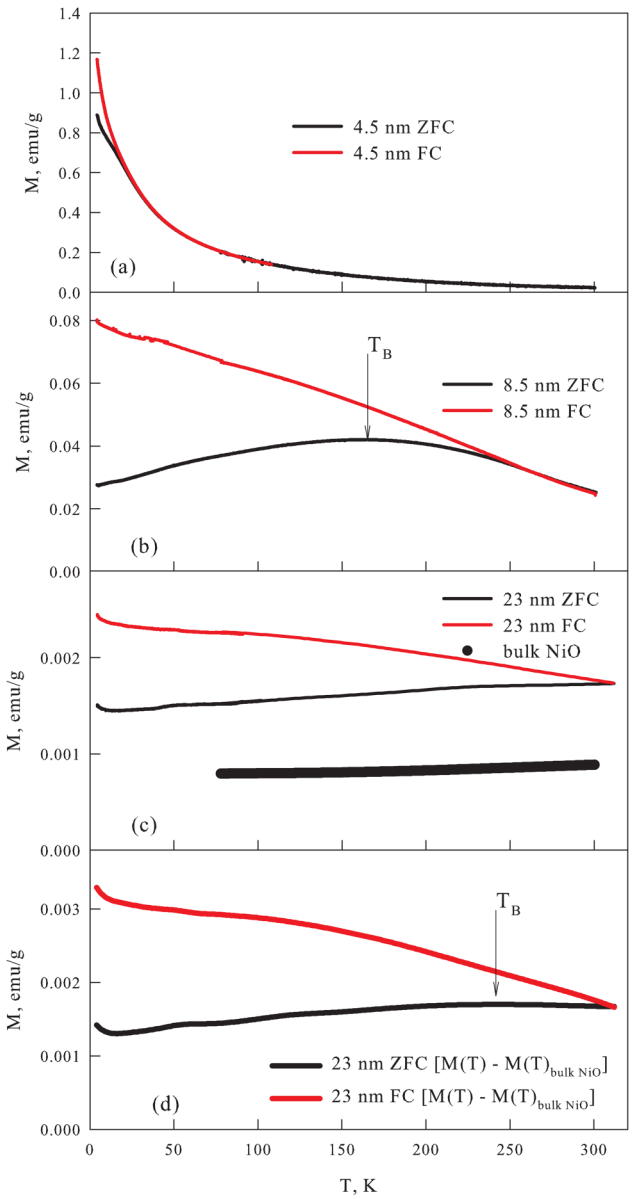

FIG. 3. Temperature dependences of magnetization for the nanoparticle and bulk NiO samples in a field of H = 1 kOe under the above-mentioned conditions. (d) M(T) dependences obtained by subtracting the M(T) dependence for the bulk NiO sample from the experimental data for 4.5-nm particles.

The $M(T)_{ZFC}$ dependence for nanoparticles 8.5 nm in size [Fig. 3(b)] has a pronounced maximum. This feature, along with the effect of the thermomagnetic on the M(T) dependences, is related to the superparamagnetic blocking of the magnetic moments of particles. For 23-nm particles, no pronounced maximum is observed; however, if we subtract the AFM contribution, i.e., the M(T) data for bulk NiO, from the M(T) data, then the resulting dependence $[M(T)_{ZFC} - M(T)_{bulk\ NiO}]$ will contain a characteristic maximum at a temperature of ~245 K [Fig. 3(d)]. For the sample consisting of smaller particles [Fig. 1(a)], the effect of thermomagnetic prehistory is observed, although there is no M

TABLE I. T_B values for NiO nanoparticles of small sizes obtained by various authors.

Size	2 nm	2 nm	2.6 nm	3 nm	3 nm	4 nm	4.5 nm	5 nm	5.3 nm	7 nm	7 nm
T_B	<2 K	<2 K	15 K	10 K	64 K	58 K	<4.2 K	5 K	150 K	5 K	15 K
Reference	38	39	40	41	42	39	This work	32	43	38	41

$(T)_{ZFC}$ maximum until 4.2 K. It is known that the value of the blocking temperature depends on several factors such as the preparation technique (degree of crystallinity), the presence of interparticle interactions, etc.[38] Table I shows a list of T_B values for NiO nanoparticles of small sizes obtained by various authors.[32,38–43] It is seen that T_B values vary sufficiently enough for similar sizes. On the other hand, the low value of the blocking temperature for 4.5-nm particles observed in the present study is in agreement with the results obtained in Refs. 32 and 38.

Thus, the blocking temperature T_B [the $M(T)_{ZFC}$ maximum] for the samples under study shift toward lower temperatures with a decrease in the NiO particle size: ~245 K for 23-nm particles, ~165 K for 8.5-nm particles, and below 4.2 K for 4.5-nm particles. At the quasistationary magnetic measurements, the T_B value is determined as $T_B \approx KV/25\,k_B$, where K is the magnetic anisotropy constant and k_B is the Boltzmann constant.[2] It is reasonable to explain a decrease in the T_B value using this expression; the detailed analysis of the effect of different factors on the T_B value of the samples of different sizes will be made elsewhere.

Figure 4 shows the M(H) dependences obtained in fields up to 250 kOe at T = 77.4 K. Note, that the M(H) dependences for 23 and 8.5-nm nanoparticles possess a relatively weak hysteresis (of order of the symbol size in Fig. 4) in the range of fields less than 30–60 kOe. This hysteresis typical for AFM nanoparticle systems[14–16,19–24,44,45] is caused by the fact that, in this case, the measuring temperature is lower than the blocking temperature ($T < T_B$). The M(H) dependence for 23-nm nanoparticles is fairly close to the linear dependence $M(H) = \chi_{bulk\ NiO} \times H$ typical of bulk NiO antiferromagnet in the whole field range. Also, it can be seen that the linear portion in the M(H) dependences for 8.5 and 4.5-nm nanoparticles is observed in strong fields. The presence of this linear portion on M(H) dependence gives evidence that the contribution of the FM subsystem to the magnetization curve becomes saturated.

It is reasonable to approximate the M(H) dependences in Fig. 4 by the functional dependence

$$M(H) = M_{FM} + C \times H, \tag{2}$$

where, according to the aforesaid, M_{FM} is the quantity characterizing the FM contribution and C is the coefficient that reflects other contributions to the magnetic susceptibility of the system. Solid lines in Fig. 4 show this approximation for the M_{FM} and C values given in Table II (the second and third rows). It can be seen that dependence (2) and the corresponding M_{FM} and C values satisfactorily describe the experimental M(H) dependence obtained in strong magnetic fields. Meanwhile, the M(H) dependences for 8.5 and 4.5-nm nanoparticles do not pass to the linear portion in fields up to 60 kOe (dashed lines in Fig. 4), so a commonly used field range up to 60 kOe does not allow us to obtain correctly the contribution of the FM subsystem.

The M_{FM} value allows us to determine the fraction $P_{FM\ Ni}$ of uncompensated nickel spins using the theoretical saturation magnetization $M_{S\ NiO}$ of fully polarized NiO ($M_{S\ NiO} \approx 148$ emu/g at $\mu_{Ni} = 2\,\mu_B$),

$$P_{FM\ Ni} = M_{FM}/M_{S\ NiO}. \tag{3}$$

Such an estimate of the fraction of free [paramagnetic (PM)] nickel spins can be obtained from the C values. They are determined by both the magnetic susceptibility of the AFM core of particles ($\chi_{bulk\ NiO}$) and the contribution of the subsystem of spins uncoupled with the AFM-ordered core[46–48] (at low temperatures,

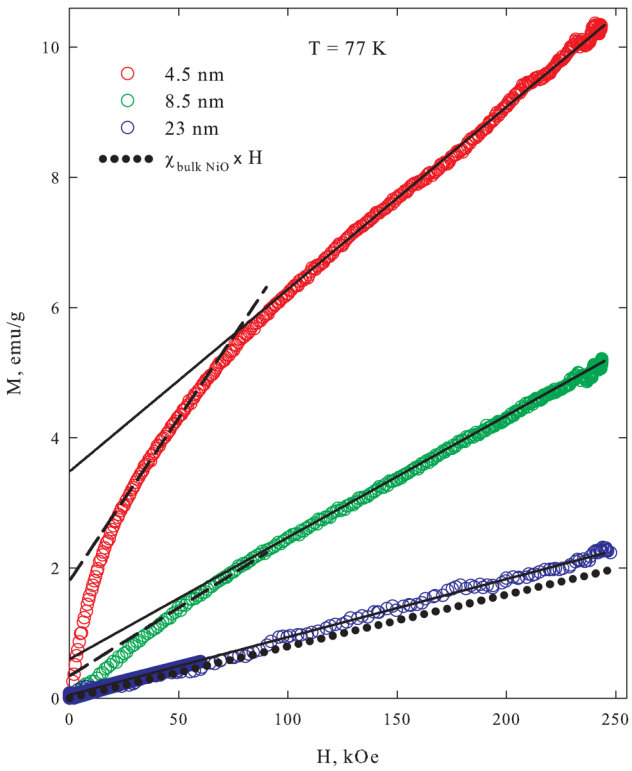

FIG. 4. Magnetization curves of the nanoparticle and bulk NiO samples. Solid lines show the linear contribution extracted using dependence (2) in the range of magnetic fields up to 250 kOe. Dashed lines illustrate noncorrect determination of the M_{FM} value using the field range up to 60 kOe.

TABLE II. Parameters of the samples and average-size particles inside them. The M_{FM} and C values were obtained by processing the data from Fig. 4 using Eq. (2). N_{Ni} is the number of nickel atoms in a particle and $N_{S\ Ni}$ is the number of nickel atoms on the surface. $N_{PM\ Ni}$ and $N_{FM\ Ni}$ are the numbers of nickel spins in a particle for the PM and FM subsystems [Eqs. (8) and (7)] and **b** is the exponent from Eq. (9).

	⟨d⟩ = 23 nm	⟨d⟩ = 8.5 nm	⟨d⟩ = 4.5 nm
M_{FM}, emu/g	0.06 (±0.005)	0.60	3.5
C, 10^{-5} emu/g Oe	0.89	1.87	2.8
N_{Ni} (in a particle)	4.51×10^5	2.28×10^4	3.38×10^3
$N_{S\ Ni}$ (on the surface)	3.53×10^4	4.82×10^3	1350
$N_{PM\ Ni}$	2.55×10^3	1.23×10^3	340
$N_{FM\ Ni}$	183	92	79
$(N_{Ni})^{\mathbf{b}}$	183	91	80
b	**b** = 0.40 (±0.015)	**b** = 0.45 (±0.01)	**b** = 0.54 (±0.01)
μ_p, μ_B	266	182	160

this subsystem can exhibit the spin-glass-like behavior[22–32]). The response of the paramagnetic (PM) subsystem can be simulated by the Brillouin function $B(\mu,H/k_BT)$: $M(H) = M_{PM} \times B(\mu,H/k_BT)$, where M_{PM} corresponds to the saturation magnetization of this spin subsystem. At T = 77 K and $\mu_{Ni} = 2\,\mu_B$ in fields up to 250 kOe, the $B(\mu,H/k_BT)$ function is field-linear: $B(\mu,H/k_BT) \approx \mu^2 H/3k_BT$. Hence, Eq. (2) can be rewritten in the form

$$M(H) = M_{FM} + M_{PM} \times \mu^2\, H/3k_BT + \chi_{bulk\ NiO} \times H. \quad (4)$$

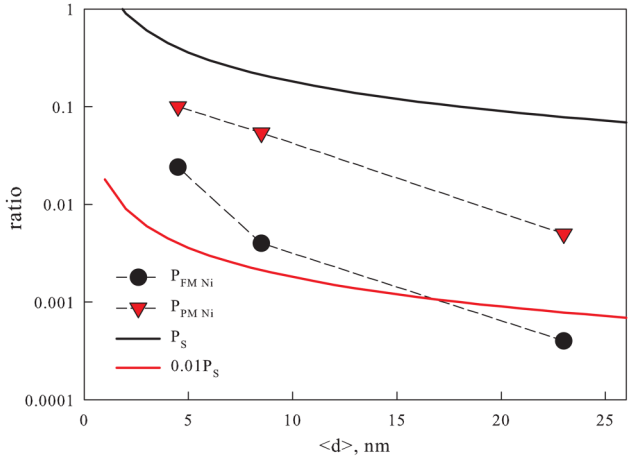

FIG. 5. Fraction $P_{FM\ Ni}$ of FM spins of the subsystem [Eq. (3)] and fraction $P_{PM\ Ni}$ of PM spins [Eq. (6)] in the total number of nickel atoms as functions of the average particle size ⟨d⟩ (symbols). Solid lines show the ratio between the number of surface atoms and the total number of nickel atoms in the NiO particle with coefficients of 1 (P_S) and 0.01 (P_S).

Using Eqs. (2) and (4), we obtain the relation for the M_{PM} value,

$$C = M_{PM} \times \mu^2\ /3k_BT + \chi_{bulk\ NiO}. \quad (5)$$

Relation (5) allows us to determine the fraction of nickel spins bound with neither the AFM core nor the FM subsystem ($P_{PM\ Ni}$). As in Eq. (3), the $P_{PM\ Ni}$ value is determined from the expression

$$P_{PM\ Ni} = M_{PM}/M_{S\ NiO}. \quad (6)$$

The obtained $P_{FM\ Ni}$ [Eq. (3)] and $P_{PM\ Ni}$ values for nanoparticles of different average sizes are presented in Fig. 5 (the logarithmic scale is along the ordinate axis). One can see a significant increase in the $P_{FM\ Ni}$ and $P_{PM\ Ni}$ values with a decrease in the particle size; i.e., the surface atoms can be a source of formation of both the PM and FM subsystems. Thus, it is reasonable to compare the behaviors of the $P_{FM\ Ni}$ and $P_{PM\ Ni}$ values with the corresponding fractions P_S of the surface atoms in a particle.

The P_S value as a function of d was calculated in the approximation of cubic particles ($V \approx d^3$) using the simple relation $P_S = 6\,(d/d_{Ni-Ni})^{-1}$ at an average interatomic spacing of $d_{Ni-Ni} \approx 0.3$ nm.[49] Figure 5 shows two calculated dependences, $P_S(d)$ and $0.01P_S(d)$; in the latter case, only 1% of the surface atoms is considered. On the one hand, there is the qualitative agreement between the behaviors of $P_{FM\ Ni}(d)$, $P_{PM\ Ni}(d)$, and $P_S(d)$: all the dependences increase with a decrease in the particle size. On the other hand, the spin fraction for the PM and FM subsystems increases faster with a decrease in the particle size than for the $P_S(d)$ dependence [or the $P_S(d)$ dependence with the coefficient smaller than unity]. Hence, the simple consideration of only the surface atoms not quite adequately describes the quantitative change of spins in the FM and PM subsystems, which form in AFM nanoparticles.

In the cubic shape particle approximation, we can obtain the number of nickel atoms in a particle with the average size $N_{Ni} = (\langle d\rangle/d_{Ni-Ni})^3$ and then use these data to determine the number of spins, also for an average-size particle, which form the FM and PM subsystems, i.e., $N_{FM\ Ni}$ and $N_{PM\ Ni}$,

$$N_{FM\ Ni} = P_{FM\ Ni} \times N_{Ni}, \quad (7)$$

$$N_{PM\ Ni} = P_{PM\ Ni} \times N_{Ni}. \quad (8)$$

Table II gives the N_{Ni}, $N_{FM\ Ni}$, and $N_{PM\ Ni}$ values, as well as the numbers of nickel atoms $N_{S\ Ni} = 6\,(d/d_{Ni-Ni})^2$ on the surface. These data together with Fig. 5 show that the number of free spins significantly (by almost an order of magnitude at ⟨d⟩ = 23 and 8.5 nm) exceeds the number of spins forming the FM subsystem. The spin of a surface atom located in the coordination nonstoichiometric for NiO can, in fact, be considered a defect. However, for the FM ordering to be established against the AFM ordering background, defects of another type should arise, at which the spin-up number is not equal to the spin-down number. Here, we may consider the number of uncompensated spins using the Néel hypothesis [Eq. (1)] based on statistical considerations. In this case, defects can be both surface and bulk.

The magnetic moment per an average-size particle can be obtained from the expression $\mu_P = N_{FM\ Ni} \times \mu_{Ni}$ (at $\mu_{Ni} = 2\mu_B$) (see Table II). In the framework of the Néel hypothesis, taking into account Eq. (1), we should, in fact, determine the **b** value in the equation

$$N_{FM\ Ni} = N_{Ni}^{\mathbf{b}}. \tag{9}$$

The obtained **b** values are given in Table II. For coarse (23-nm) particles, the model Néel hypothesis describes the number of uncompensated spins at the exponent **b** values intermediate between the idealized case of only surface defects and bulk defects in a particle. The **b** value increases with a decrease in the particle size and approaches 1/2, which is reasonable to attribute to the occurrence of defects in the bulk of a particle.

We would like to emphasize an interesting feature, which points out the different roles of defects in the AFM and ferrimagnetic nanoparticles. It is well known that with a decrease in the size of ferrimagnetic oxide nanoparticles, the specific saturation magnetization M_S decreases.[50–55] This is attributed to the presence of a magnetically dead surface layer with thickness a up to ~1.5 nm. The M_S value can be determined using the expression $M_S = M_{S\ bulk}(1 - 2a/d)^3$,[48] where $M_{S\ bulk}$ is the saturation magnetization of the bulk material. This expression can be rewritten in the form

$$M_S^{1/3} = M_{S\ bulk}\ (1 - 2a/d). \tag{10}$$

The authors of Ref. 53 investigated a series of samples containing γ-Fe_2O_3 nanoparticles of different sizes and, based on the results obtained and the data reported in other works, showed that Eq. (10) is valid for the experimental data at $a \sim 1$ nm for the particles with a size of $d > 3$ nm. Figure 6 schematically shows

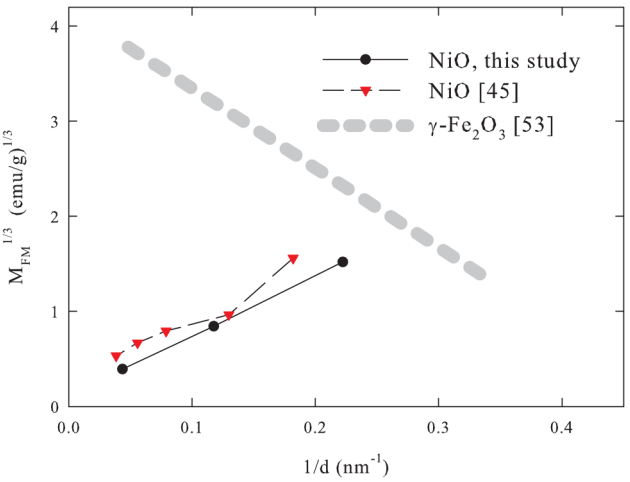

FIG. 6. Dependences of $M_{FM}^{1/3}$ on 1/d for NiO nanoparticles plotted using our results and data from Ref. 45 and dependence of $M_S^{1/3}$ on 1/d for ferrimagnetic γ-Fe_2O_3 nanoparticles plotted using the data from Ref. 53 [Eq. (10)].

dependence (10) at $a = 1$ nm[53] in coordinates $M_S^{1/3}$ and 1/d (dashed line), which describes the experimental results for γ-Fe_2O_3 nanoparticles (for bulk γ-Fe_2O_3, $M_S \approx 76$ emu/g). In addition, Fig. 6 presents the data for NiO obtained in our investigations; in our case, this is the dependence of $M_{FM}^{1/3}$ on 1/d. One can see a drastic difference between the behaviors of the saturation magnetization for AFM and ferrimagnetic nanoparticles. The experimental data on NiO nanoparticles from Ref. 45 plotted in Fig. 6 confirm the aforesaid, although the M_{FM} values reported in Ref. 45 were apparently somewhat overestimated due to the narrower magnetic field range used in the experiment.

The $M_{FM}(d)$ dependence for AFM nanoparticles can be obtained also using Eqs. (3), (7), and (9): $M_{FM} = M_{S\ NiO}(N_{FM}/N_{Ni}) = M_{S\ NiO}(N_{Ni}^{\mathbf{b}}/N_{Ni}) = M_{S\ NiO}(d/d_{Ni-Ni})^{3(\mathbf{b}-1)}$; therefore,

$$M_{FM}^{1/3} = M_{S\ NiO}^{1/3}(d/d_{Ni-Ni})^{(\mathbf{b}-1)}. \tag{11}$$

The **b** value, however, depends on the particle size, and the variation can generally range from 1/3 to 2/3. Therefore, we do not expect a strict functional $M_{FM}(d)$ [and $M_{FM}^{1/3}(1/d)$] power dependence. The data presented in Fig. 6, which were obtained in this work, are satisfactorily described by the dependence $M_{FM}^{1/3} = 240^{1/3}(1/d) + 0.13$. This dependence contains a constant term, which has no physical meaning, since, at small 1/d values, M_{FM} must tend to zero, and, in addition, the quantity 240 emu/g is higher than the theoretical value for fully polarized NiO (148 emu/g). This is indicative of the fact that the linear dependence of $M_{FM}^{1/3}$ on 1/d observed in NiO nanoparticles (Fig. 6) follows from the **b** variation [in our case, the **b** value changes from 0.4 to 0.54 (see Table II) in Eq. (11)]. Thus, functional dependence (11) and the observed **b** growth with a decrease in the NiO nanoparticle size explain the behavior of the parameter M_{FM} in Fig. 6, although the data presented in Fig. 6 speak about the approximately linear dependence of $M_{FM}^{1/3}$ on 1/d.

According to Eq. (1), the magnetic moment μ_P of an AFM particle decreases with the particle size (see Table II). However, AFM particles several nanometers in size are an alternative to ferrimagnetic particles in the saturation magnetization and magnetic moment, which, certainly, broadens, the range of possible applications of AFM particles.

IV. CONCLUSIONS

Thus, we examined the magnetic properties of a series of samples formed by nickel oxide nanoparticles with average sizes from 23 to 4.5 nm. The technique used for measuring the magnetization in strong pulsed magnetic fields allowed us to correctly extract the contributions of the unbound (free) spin subsystem and ferromagnetic subsystem forming in AFM NiO nanoparticles due to the partial decompensation of spins. The fraction of uncompensated spins (FM subsystem) increases with a decrease in the nanoparticle size from 0.04% for 23-nm particles to 2.4% for 4.5-nm particles. The Néel relation $\mu_P \sim \mu \cdot N^{\mathbf{b}}$ is valid at the exponents **b** of 0.4, 0.45, and 0.54 for particles with average sizes of 23, 8.5, and 4.5 nm, respectively. This is indicative of a decisive role of defects in the formation of the FM subsystem in AFM NiO nanoparticles. As the particle size decreases, the defects in the bulk of particles

start playing an increasing role, along with the surface defects. Then, the saturation magnetization of the FM component becomes comparable with the value for ferrimagnetic oxide particles of similar sizes.

ACKNOWLEDGMENTS

We are grateful to S. V. Semenov for help and A. D. Balaev for fruitful discussions. The TEM study was carried out on a facility of the Resource Sharing Center, Krasnoyarsk Scientific Center, Siberian Branch, Russian Academy of Sciences.

FUNDING INFORMATION

This study was supported by the Ministry of Science and Higher Education of the Russian Federation and by the Russian Foundation for Basic Research, Government of the Krasnoyarsk Territory, and Krasnoyarsk Territorial Foundation for Support of Scientific and R&D Activities, project: "Magnetic Reversal of Magnetic Nanoparticles in Strong Pulsed Magnetic Fields—A New Approach to the Study of Dynamic Effects Associated with the Magnetization of Magnetic Nanoparticles," Project No. 18-42-240012.

REFERENCES

[1]L. Néel, C. R. Acad. Sci. Paris **252**, 4075 (1961).
[2]S. Mørup, D. E. Madsen, C. Frandsen, C. R. H. Bahl, and M. F. Hansen, J. Phys. Condens. Matter **19**, 213202 (2007).
[3]Y. L. Raikher and V. I. Stepanov, J. Phys. Condens. Matter. **20**, 204120 (2008).
[4]B. Issa, I. M. Obaidat, B. A. Albiss, and Y. Haik, Int. J. Mol. Sci. **14**, 21266 (2013).
[5]K. Dobretsov, S. Stolyar, and A. Lopatin, Acta Otorhinolaryngol. Ital. **35**(2), 97 (2015).
[6]S. V. Stolyar, D. A. Balaev, V. P. Ladygina *et al.*, J. Supercond. Nov. Magn. **31**, 2297 (2018).
[7]S. A. Makhlouf, F. T. Parker, and A. E. Berkowitz, Phys. Rev. B **55**, R14717 (1997).
[8]J. G. E. Harris, J. E. Grimaldi, D. D. Awschalom, A. Chilero, and D. Loss, Phys. Rev. B **60**, 3543 (1999).
[9]M. S. Seehra, V. S. Babu, A. Manivannan, and J. W. Lynn, Phys. Rev. B **61**, 3513 (2000).
[10]C. Gilles, P. Bonville, K. K. W. Wong, and S. Mann, Eur. Phys. J. B **17**, 417 (2000).
[11]C. Gilles, P. Bonville, H. Rakoto, J. M. Broto, K. K. W. Wong, and S. Mann, J. Magn. Magn. Mater. **241**, 430 (2002).
[12]A. Punnoose, T. Phanthavady, M. S. Seehra, N. Shah, and G. P. Huffman, Phys. Rev. B **69**, 054425 (2004).
[13]N. J. O. Silva, V. S. Amaral, and L. D. Carlos, Phys. Rev. B **71**, 184408 (2005).
[14]D. A. Balaev, A. A. Krasikov, A. A. Dubrovskii, S. V. Semenov, O. A. Bayukov, S. V. Stolyar, R. S. Iskhakov, V. P. Ladygina, and L. A. Ishchenko, J. Exp. Theor. Phys. **119**(3), 479 (2014).
[15]D. A. Balaev, A. A. Krasikov, A. A. Dubrovskiy, S. I. Popkov, S. V. Stolyar, O. A. Bayukov, R. S. Iskhakov, V. P. Ladygina, and R. N. Yaroslavtsev, J. Magn. Magn. Mater. **410**, 171 (2016).
[16]D. A. Balaev, A. A. Krasikov, S. V. Stolyar, R. S. Iskhakov, V. P. Ladygina, R. N. Yaroslavtsev, O. A. Bayukov, A. M. Vorotynov, M. N. Volochaev, and A. A. Dubrovskiy, Phys. Solid State **58**(2), 1782 (2016).
[17]J. T. Richardson, D. I. Yiagas, B. Turk, K. Forster, and M. V. Twigg, J. Appl. Phys. **70**, 6977 (1991).
[18]S. D. Tiwari and K. P. Rajeev, Solid State Commun. **152**, 1080 (2012).
[19]C. R. H. Bahl, M. F. Hansen, T. Pedersen, S. Saadi, K. H. Nielsen, B. Lebech, and S. Mørup, J. Phys. Condens. Matter **18**, 4161–4175 (2006).
[20]M. Vasquez-Mansilla, R. D. Zysler, C. Arciprete, M. I. Dimitrijewits, C. Saragovi, and J. M. Greneche, J. Magn. Magn. Mater. **204**, 29 (1999).
[21]R. D. Zysler, M. Vasquez Mansilla, and D. Fiorani, Eur. Phys. J. B **41**, 171 (2004).
[22]A. A. Lepeshev, I. V. Karpov, A. V. Ushakov, D. A. Balaev, A. A. Krasikov, A. A. Dubrovskiy, D. A. Velikanov, and M. I. Petrov, J. Supercond. Nov. Magn. **30**, 931 (2017).
[23]R. H. Kodama, A. E. Berkowitz, E. J. McNiff, and S. Foner, J. Appl. Phys. **81**, 5552 (1997).
[24]R. H. Kodama and A. E. Berkowitz, Phys. Rev. B **59**, 6321 (1999).
[25]Y. A. Koksharov, S. P. Gubin, I. D. Kosobudsky, G. Y. Yurkov, D. A. Pankratov, L. A. Ponomarenko, M. G. Mikheev, M. Beltran, Y. Khodorkovsky, and A. M. Tishin, Phys. Rev. B **63**, 012407 (2000).
[26]E. Winkler, R. D. Zysler, M. Vasquez Mansilla, and D. Fiorani, Phys. Rev. B **72**, 132409 (2005).
[27]N. J. O. Silva, A. Millan, F. Palacio, E. Kampert, U. Zeitler, and V. S. Amaral, Phys. Rev. B **79**, 104405 (2009).
[28]M. S. Seehra, V. Singh, X. Song, S. Bali, and E. M. Eyring, J. Phys. Chem. Solids **71**, 1362 (2010).
[29]M. Tadić, M. Panjan, D. Marković, I. Milošević, and V. Spasojević, J. Alloys Compd. **509**, 7134 (2011).
[30]S. D. Tiwari and K. P. Rajeev, Phys. Rev. B **72**, 104433 (2005).
[31]D. Nikolić, M. Panjan, G. R. Blake, and M. Tadić, J. Eur. Ceram. Soc. **35**, 3843 (2015).
[32]M. Tadic, D. Nikolic, M. Panjan, and G. R. Blake, J. Alloys Compd. **647**, 1061 (2015).
[33]D. A. Balaev, A. A. Dubrovskiy, A. A. Krasikov, S. I. Popkov, A. D. Balaev, K. A. Shaikhutdinov, V. L. Kirillov, and O. N. Martyanov, Phys. Solid State **59**, 1547 (2017).
[34]D. A. Balaev, S. I. Popkov, A. A. Krasikov, A. D. Balaev, A. A. Dubrovskiy, S. V. Stolyar, R. N. Yaroslavtsev, V. P. Ladygina, and R. S. Iskhakov, Phys. Solid State **59**, 1940 (2017).
[35]R. P. Guertin, N. Harrison, Z. X. Zhou, S. McCall, and F. Drymiotis, J. Magn. Magn. Mater. **308**, 97 (2007).
[36]S. I. Popkov, A. A. Krasikov, D. A. Velikanov, V. L. Kirillov, O. N. Martyanov, and D. A. Balaev, J. Magn. Magn. Mater. **483**, 21–26 (2019).
[37]J. R. Singer, Phys. Rev. **104**, 929 (1956).
[38]J. Park, E. Kang, S. U. Son, H. M. Park, M. K. Lee, J. Kim, K. W. Kim, H.-J. Noh, J.-H. Park, C. J. Bae, J.-G. Park, and T. Hyeon, Adv. Mater. **17**, 429 (2005).
[39]N. Rinaldi-Montes, P. Gorria, D. Martínez-Blanco, A. B. Fuertes, L. Fernández Barquín, I. Puente-Orench, and J. A. Blanco, Nanotechnology **26**, 305705 (2015).
[40]T. Tajiri, S. Saisho, M. Mito, H. Deguchi, K. Konishi, and A. Kohno, J. Phys. Chem. **119**, 1194 (2015).
[41]M. Ghosh, K. Biswas, A. Sundaresan, and C. N. R. Rao, J. Mater. Chem. **16**, 106 (2006).
[42]E. Winkler, R. D. Zysler, M. Vasquez Mansilla, D. Fiorani, D. Rinaldi, M. Vasilakaki, and K. N. Trohidou, Nanotechnology **19**, 185702 (2008).
[43]S. A. Makhlouf, F. T. Parker, F. E. Spada, and A. E. Berkowitz, J. Appl. Phys. **81**, 5561 (1997).
[44]S. Baran, A. Hoser, B. Penc, and A. Szytuła, Acta Pol. A **129**, 35 (2016).
[45]S. A. Makhlouf, H. Al-Attar, and R. H. Kodama, Solid State Commun. **145**, 1 (2008).
[46]Another source of the additional field-linear contribution to the total magnetization can be the superantiferromagnetism, see Refs. 47 and 48, which should be specially analyzed.[11,27]
[47]L. Néel, C. R. Acad. Sci. Paris **253**, 203 (1961).
[48]L. Néel, C. R. Acad. Sci. Paris **253**, 1286 (1961).
[49]W.-L. Jang, Y.-M. Lu, W.-S. Hwang, T.-L. Hsiung, and H. P. Wang, Appl. Phys. Lett. **94**, 062103 (2009).

[50]G. F. Goya, T. S. Berquó, F. C. Fonseca, and M. P. Morales, J. Appl. Phys. **94**, 3520 (2003).
[51]P. Dutta, S. Pal, M. S. Seehra, N. Shah, and G. P. Huffman, J. Appl. Phys. **105**, 07B501 (2009).
[52]S. Ayyappan, G. Panneerselvam, M. P. Antony, N. V. Rama Rao, N. Thirumurugan, A. Bharathi, and J. Philip, J. Appl. Phys. **109**, 084303 (2011).
[53]A. Millan, A. Urtizberea, N. J. O. Silva, F. Palacio, V. S. Amaral, E. Snoeck, and V. Serin, J. Magn. Magn. Mater. **312**, L5 (2007).
[54]V. L. Kirillov, D. A. Balaev, S. V. Semenov, K. A. Shaikhutdinov, and O. N. Martyanov, Mater. Chem. Phys. **145**, 75 (2014).
[55]S. Mosivand, L. M. A. Monzon, K. Ackland, I. Kazeminezhad, and J. M. D. Coey, J. Phys. D Appl. Phys. **47**, 055001 (2014).